catalysts

MDPI

Article

Biodesulfurization of Dibenzothiophene by Decorating *Rhodococcus erythropolis* IGTS8 Using Montmorillonite/Graphitic Carbon Nitride

Nika Yavani Hasanbeik [1], Mehrab Pourmadadi [2], Azam Ghadami [1,*], Fatemeh Yazdian [3,*], Abbas Rahdar [4,*] and George Z. Kyzas [5,*]

[1] Department of Chemical and Polymer Engineering, Central Tehran Branch, Islamic Azad University, Tehran 13117773591, Iran
[2] Department of Biotechnology, School of Chemical Engineering, College of Engineering, University of Tehran, Tehran 14179-35840, Iran
[3] Department of Life Science Engineering, Faculty of New Sciences and Technologies, University of Tehran, Tehran 14179-35840, Iran
[4] Department of Physics, University of Zabol, Zabol 98613-35856, Iran
[5] Department of Chemistry, International Hellenic University, 65404 Kavala, Greece
* Correspondence: a.ghadami@iauctb.ac.ir (A.G.); yazdian@ut.ac.ir (F.Y.); a.rahdar@uoz.ac.ir (A.R.); kyzas@chem.ihu.gr (G.Z.K.)

Abstract: Fossil fuels are the main sources of human energy, but their combustion releases toxic compounds of sulfur oxide. In the oil industry, using the optimal methods to eliminate sulfur compounds from fossil fuels is a very important issue. In this study, the performance of montmorillonite/graphitic carbon nitride (a new hybrid nanostructure) in increasing the biodesulfurization activity of *Rhodococcus erythropolis* IGTS8 was investigated. X-ray diffraction, Fourier-transform infrared spectroscopy, field emission scanning electron microscopy and transmission electron microscopy were used for the characterization of the nanoparticles. The effective factors in this process were determined. Optimum conditions for microorganisms were designed using the Design Expert software. Experiments were performed in a flask. The results indicated that the biodesulfurization activity of a microorganism in the presence of the nanostructure increases by 52%. In addition, in the presence of the nanostructure, the effective factors are: 1. concentration of the nanostructure; 2. concentration of sulfur; 3. cell concentration. In the absence of the nanostructure, the only effective factor is the concentration of sulfur. Through analysis of variance, the proposed models were presented to determine the concentration of the 2-hydroxy biphenyl produced by the microorganisms (biodesulfurization activity) in the presence and absence of the nanostructure. The proposed models were highly acceptable and consistent with experimental data. The results of a Gibbs assay showed that the biodesulfurization efficiency of in the presence of the nanostructure was increased by about 52%, which is a very satisfactory result. The biodesulfurization activity of decorated cells in a bioreactor showed a significant increase compared with nondecorated cells. Almost a two-fold improvement in biodesulfurization activity was obtained for decorated cells compared with free cells.

Keywords: biodesulfurization; dibenzothiophene; montmorillonite; graphitic carbon nitride

Citation: Hasanbeik, N.Y.; Pourmadadi, M.; Ghadami, A.; Yazdian, F.; Rahdar, A.; Kyzas, G.Z. Biodesulfurization of Dibenzothiophene by Decorating *Rhodococcus erythropolis* IGTS8 Using Montmorillonite/Graphitic Carbon Nitride. *Catalysts* **2022**, *12*, 1450. https://doi.org/10.3390/catal12111450

Academic Editors: Xiaofeng Chen, Ihsanullah Ihsanullah and Helder T. Gomes

Received: 25 September 2022
Accepted: 14 November 2022
Published: 17 November 2022

1. Introduction

Fossil fuels provide 85% of human energy needs [1,2]. Sulfur is the most abundant element in oil after carbon and hydrogen [3]. The release of sulfur oxides that have detrimental effects on human health (respiratory diseases), the environment (acid rain) and economics (catalyst corrosion and poisoning) is the result of the combustion of sulfur-containing compounds in fossil fuels [3–5].

Hence, the main issue of the world today is the use of environmentally friendly fuels. A serious challenge for refineries is to turn low-quality crude oil to high-quality final

products [6]. Different desulfurization methods are available to eliminate the sulfur in oil and petroleum products. Hydrodesulfurization (HDS) is more commonly used in refineries. This process is a common method for decreasing the amount of sulfur in fuel by using a metal catalyst to reduce the amount of sulfur organic compounds to a lower level [7]. This process is not suitable for the elimination of complex heterocyclic compounds of sulfur such as BT (benzothiophene), DBT (dibenzothiophene), or 4, 6-DMDBT (dimethyl dibenzothiophene). Thus, they remain in the oil and its products [8]. Another problem with this process is the need for high temperature and pressure because the sulfur atoms in sulfur compounds are converted to hydrogen sulfide at high pressure and temperature in the presence of hydrogen gas and metal catalysts such as $CoMo/Al_2O_3$ or ($NiMo/Al_2O_3$). Depending upon the required degree of desulfurization and the kind of hydrocarbon, desulfurization can occur at pressures of 150 to 250 Psi of hydrogen and at temperatures of 425–200 °C [4,9]. In such cases, the amount of sulfur may be reduced from 1–5% to 0.1%. Biodesulfurization does not have these problems. This process is done at low pressure and temperature conditions that help to save energy, and it is a complementary process for deep hydrodesulfurization [9]. Specific microorganisms help to remove sulfur from crude oil in biodesulfurization. The metabolic ability of microorganisms is one of the reasons for the application of biotechnology methods in many scientific fields [10]. Bacteria have received the most attention among all microorganisms due to their unique characteristics (ability to grow and size) [3]. These microorganisms eliminate the organic Sulfur compounds from petroleum components without decomposing the carbon skeleton [11]. Among bacterial species, many studies have pointed to the activity and high selectivity of *Rhodococcus erythropolis* IGTS8 in removing sulfur from organic compounds in crude oil [12,13]. Members of this bacterial species are used as organic materials due to the special structure of their cell walls and their appropriate biochemical characteristics for the biological degradation of organic compounds and industry [11,14]. *Rhodococcus erythropolis* IGTS8 is capable of the selective oxidation of sulfur atoms from sulfur-containing heterocyclic compounds through the 4S pathway without metabolizing the carbon skeleton [15].

In the 4S pathway, the first step involves the conversion of DBT to DBT sulfoxide (DBTO), and then the DBTO is converted to DBT sulfone ($DBTO_2$). The first and the second steps are catalyzed by the synchronous action of a DBT-monooxygenase (DszC) and an NADH-flavin mononucleotide oxidoreductase (DszD) supplying the needed $FMNH_2$. The third step involves the conversion of DBT-sulfone to 2-hydroxybiphenyl-2-sulfinic acid (HBPS) by the synchronous action of a DBT-sulfone monooxygenase (DszA) and DszD. The fourth step involves the conversion of HBPS to 2-hydroxybiphenyl and sulfite by the synchronous action of sulfinate desulfinase (DszB) [16].

There are two main groups of sulfur in crude oil [3]. A higher percentage of sulfur compounds are organic compounds [17]. DBT is a common organosulfur compound that is found in a variety of fuels, and because this substance is more resistant to the hydrodesulfurization process than the other thiophene sulfides it is widely regarded as a model compound for biodesulfurization [18,19]. In prior research, Goubin et al. coated the microbial cells of *Pseudomonas delafieldii* with Fe_3O_4 nanoparticles and immobilized them by the external application of a magnetic field. They showed that the coated cells and the free cells had the same desulfurization activity. The coated cells with Fe_3O_4 nanoparticles had higher desulfurization activity compared with the immobilized cells on celite [20]. Ansari et al. investigated the desulfurization activity of coated cells using magnetic Fe_3O_4 nanoparticles. The size of the magnetic Fe_3O_4 nanoparticles was 45–50 nm. They showed that the decorated cells had a 56% higher desulfurization activity compared with the nondecorated cells [21]. Zhang et al. investigated the biodesulfurization activity of nano-γ-Al_2O_3 particles assembled on magnetic immobilized *Rhodococcus erythropolis* LSSE8-1-vgb. They showed that the biodesulfurization activity was enhanced by 20% when the amount ratio of magnetic nanoparticles to nano-γ-Al_2O_3 particles was 1:5 (g/g) [22]. Bardania et al. investigated the application of Fe_3O_4 nanoparticles to the separation of *Rhodococcus erythropolis* FMF and *R. erythropolis* IGTS8 and their influence on desulfurization activity.

They showed that the Fe_3O_4 nanoparticles had no effect on desulfurization activity [13]. Etemadi et al. investigated the influence of starch/Fe_3O_4 and starch/Fe nanoparticles on the biodesulfurization efficiency of microbial cells of Bacillus thermoamylovorans. The size of the starch/Fe_3O_4 nanoparticles was 20 nm, and the size of the starch/Fe nanoparticles was 30–40 nm. They showed that the cells immobilized by the starch/Fe_3O_4 and starch/Fe nanoparticles had a higher biodesulfurization efficiency, i.e., by about 10% and 22%, respectively [23]. Rahpeyma et al. investigated the biodesulfurization of dibenzothiophene by two bacterial strains of *Rhodococcus erythropolis* IGTS8 and Pseudomonas aeruginosa PTSOX4 in cooperation with Fe_3O_4, ZnO and CuO nanoparticles. They showed that the biodesulfurization capacity of the ZnO nanoparticles was higher than that of the Fe_3O_4 and CuO nanoparticles [24]. In another study, Rahpeyma et al. investigated the biodesulfurization activity of *Rhodococcus erythropolis* IGTS8 cells coated with functionalized magnetic iron oxide nanoparticles. They showed that the coated cells had a higher desulfurization ability compared with the uncoated cells [11]. There is an obstacle which limits the application of biodesulfurization in many cases: the limited bioavailability of organosulfur compounds in the oil phase to the microbial culture in the aqueous phase, which affects the biodesulfurization activity of the microbial cells and leads to a low efficiency of this process [25,26]. The use of nanostructures in order to solve this problem has been mentioned in many studies [12,21,24]. The results of different studies have not shown a significant increase in biodesulfurization efficiency, so we decided to use another nanostructure. The suitable properties of montmorillonite for oxidative and adsorptive desulfurization have shown good results. Evidence of this includes research conducted in different years. In various experiments, Ahmad et al. investigated the adsorptive desulfurization of diesel oil and kerosene using montmorillonite. Their results showed that montmorillonite clay can be used effectively in adsorptive desulfurization [27]. Montmorillonite is a type of smectite nanostructure that is inexpensive, environmental friendly, non-toxic and highly accessible compared with other smectite nanoclays [28–31]. This material has a 2:1 layered structure, consisting of two tetrahedral layers of silicate and an octahedral layer of alumina, in which the octahedral layer is sandwiched between the two tetrahedral layers [32–35]. Studies on montmorillonite show the power of this nanoclay for the fabrication of catalysts, polymer nanocomposites and adsorbents [33]. Due to the fact that montmorillonite is hydrophobic, the hydration of this material causes the galleries to expand and the clay to swell [32]. Due to the hydrophilic nature of montmorillonite, this nanoclay is normally an inert adsorbent for organic compounds [36–39]. One of the important research achievements is that a nanocomposite of montmorillonite, along with other materials, has shown good catalytic activity. Among these studies, we mention Rezvani and Khandan (2018). The increase in the rate of oxidative desulfurization by $FeW_{11}V$/CTAB-MMT nanocomposite was evaluated, and the results showed that the desulfurization rates of BT and DBT with applied nanocomposites at 35 °C after 1 h were more than 97% [40]. In the present study, various studies were investigated to synthesize a new nanocomposite of montmorillonite with a higher specific surface area to increase the access and uptake of nutrients by microorganisms and ultimately improve the desulfurization performance. The results showed acceptable activity by g-C_3N_4 (graphitic carbon nitride) in oxidative desulfurization. For example, Wong et al. evaluated the increase in the rate of oxidative desulfurization of a model molecule (dibenzothiophene) using a titanium dioxide/graphitic carbon nitride composite. The removal efficiency reached 98.9% [41]. In a study by Rongxiang et al., the performance of a tungsten oxide/graphitic carbon nitride composite in the oxidation desulfurization of dibenzothiophene was evaluated, and the results showed a high performance (91.2%) of this material under optimal conditions [42]. MMT with g-C_3N_4 were used to form a unique nanocomposite. Graphitic carbon nitride is an acclaimed polymer composed of carbon and nitrogen (band gap = 2.7 eV) [43]. The advantages of g-C_3N_4 are its adequate biocompatibility, low density and high chemical stability. Consequently, it performs well in various applications, e.g., as a catalyst, a membrane or a catalyst carrier [42,44], and due to its economical and simplistic preparation methods, it has become a significant sub-

stance [45,46]. Graphitic carbon nitride consists of triazine (C_3N_3) or tri-S-triazine (C_6N_7) units, and between the layers there are van der Waals forces [46].

In the present study, a new hybrid nanostructure called montmorillonite/graphitic carbon nitride was synthesized, and its performance in improving the activity of *Rhodococcus erythropolis* IGTS8 in the desulfurization of dibenzothiophene was investigated. For this purpose, the experimental design was performed using the Design Expert software and the optimization of the operational parameters affecting the performance of the nanostructure in the biodesulfurization activity of *Rhodococcus erythropolis* IGTS8 was carried out. Through analysis of variance, the proposed models were obtained to determine the concentration of 2-hydroxy biphenyl produced by the microorganism (i.e., to determine the desulfurization activity) in the presence and absence of the nanostructure.

2. Results and Discussion

2.1. TEM and FESEM Analysis

The TEM images of the graphitic carbon nitride are represented in Figure 1A. The graphitic carbon nitride is composed of mushy and small layered nanosheets with non-uniform (asymmetrical) forms. The FESEM images of the MMT/g-C_3N_4 nanostructure are represented in Figure 1B. The MMT sheets have a smooth and layered surface. These sheets also have uniform shapes. The primary structure of the g-C_3N_4 has changed because of its blending with the MMT. The graphitic carbon nitride is properly attached to the surface of the MMT and covers it. Additionally, these materials are well combined with each other. When the synthesized g-C_3N_4 nanosheets combine with the MMT, they appear as agglomerate and have a completely spherical structure. In this research, we did not have TEM images of the MMT/g-C_3N_4 nanostructure because a TEM is a very large and quite expensive piece of electron microscopy machinery. Due to the complexity of the item, special training is required not only to operate the product, but also to be able to accurately analyze the data that the sample imaging provides. Aside from the operation of the product, there can be laborious work involved in preparing a sample for analysis. Firstly, the nature of the sample needs to be taken into consideration. Specifically, will the sample be able to withstand the vacuum chamber? The sample needs to be sliced thin enough for electrons to pass through, but also be able to withstand the process of analysis.

2.2. XRD and FTIR Analysis

Peaks at 2θ = 20.1(100), 28.5(005), 35.6(110), 54.25(210), 62.35(300), 73.65(221) and 76.9(310) were observed in the X-ray diffraction pattern of the MMT [47]. In the X-ray diffraction pattern analysis, sharp, high-intensity peaks indicate the formation of nanoparticles with a fine crystalline structure. The X-ray diffraction pattern of the ultra-thin g-C_3N_4 nanosheets shows a sharp diffraction peak at 27.8°, which originated from the (002) represented inter-layer stacking of the aromatic units [48]. In the XRD pattern of the montmorillonite/graphitic carbon nitride there is a sharp and high-intensity peak at 27.75°, which is similar to that of the XRD of the graphitic carbon nitride. Figure 2A represents the XRD pattern of the MMT, graphitic carbon nitride and montmorillonite/graphitic carbon nitride.

In MMT, the bending vibrations of Si-O-Si, Si-O-Al, Al-Mg-OH and Al-Al-OH are observed at 467 cm^{-1}, 523 cm^{-1}, 796 cm^{-1} and 914 cm^{-1}, respectively. The stretching vibration of Si-O is observed at 993 cm^{-1} and 1113 cm^{-1}. The bands of 1635 cm^{-1} and 3405 cm^{-1} belong to the bending and stretching vibration of the group of O-H of the adsorbed H_2O. Stretching vibrations corresponding to the octahedral cations are observed at 3631 cm^{-1} and 3694 cm^{-1}. The band of 3444 cm^{-1} belongs to the group of O-H, which indicates presence of water between the layers of the MMT [49,50]. The g-C_3N_4 nanosheets have a sharp and high-intensity band at 810 cm^{-1}, and it shows a kind of bending vibration of the C_3N_3 rings in these nanosheets. Several characteristic bands at 1242 cm^{-1}, 1323 cm^{-1}, 1414 cm^{-1}, 1570 cm^{-1} and 1637 cm^{-1} result in stretching modes of the C-N and C = N in the CN heterocycles. The broad absorption bands from approximately 3000 cm^{-1} to 3300 cm^{-1} pertain to the N-H stretching vibration of the NH groups or residual NH_2 and

the stretching vibration of the group of O-H of the adsorbed H_2O [48]. As can be seen, the MMT/g-C_3N_4 nanostructure has similar peaks to g-C_3N_4. Figure 2B shows the FTIR spectroscopy of the MMT, g-C_3N_4 and MMT/g-C_3N_4.

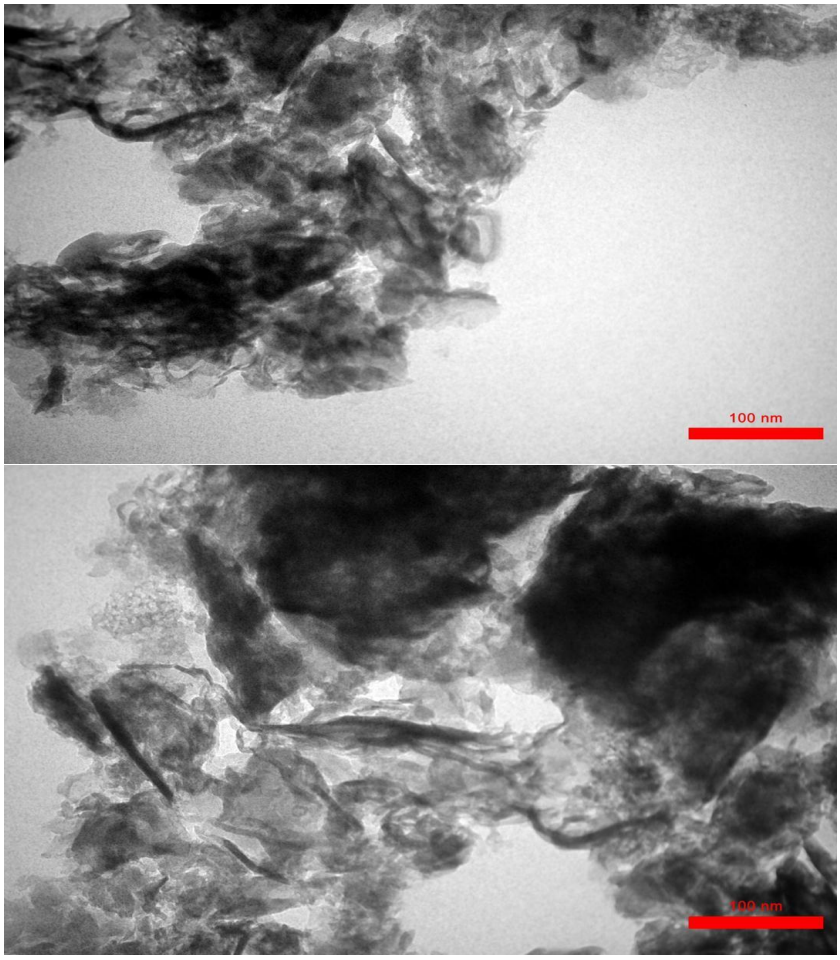

(**A**)

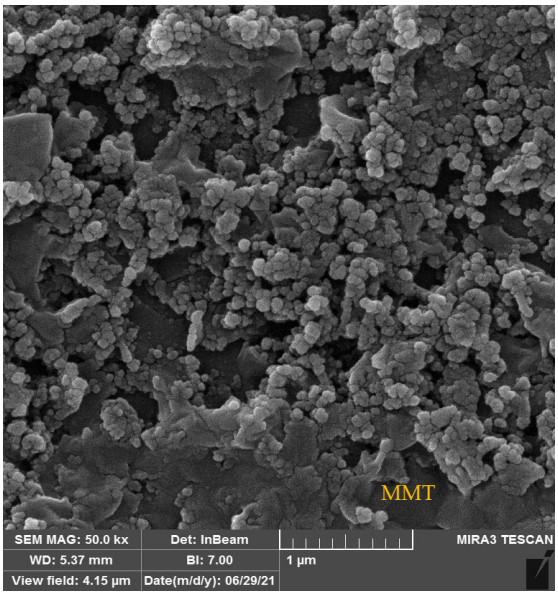

Figure 1. *Cont.*

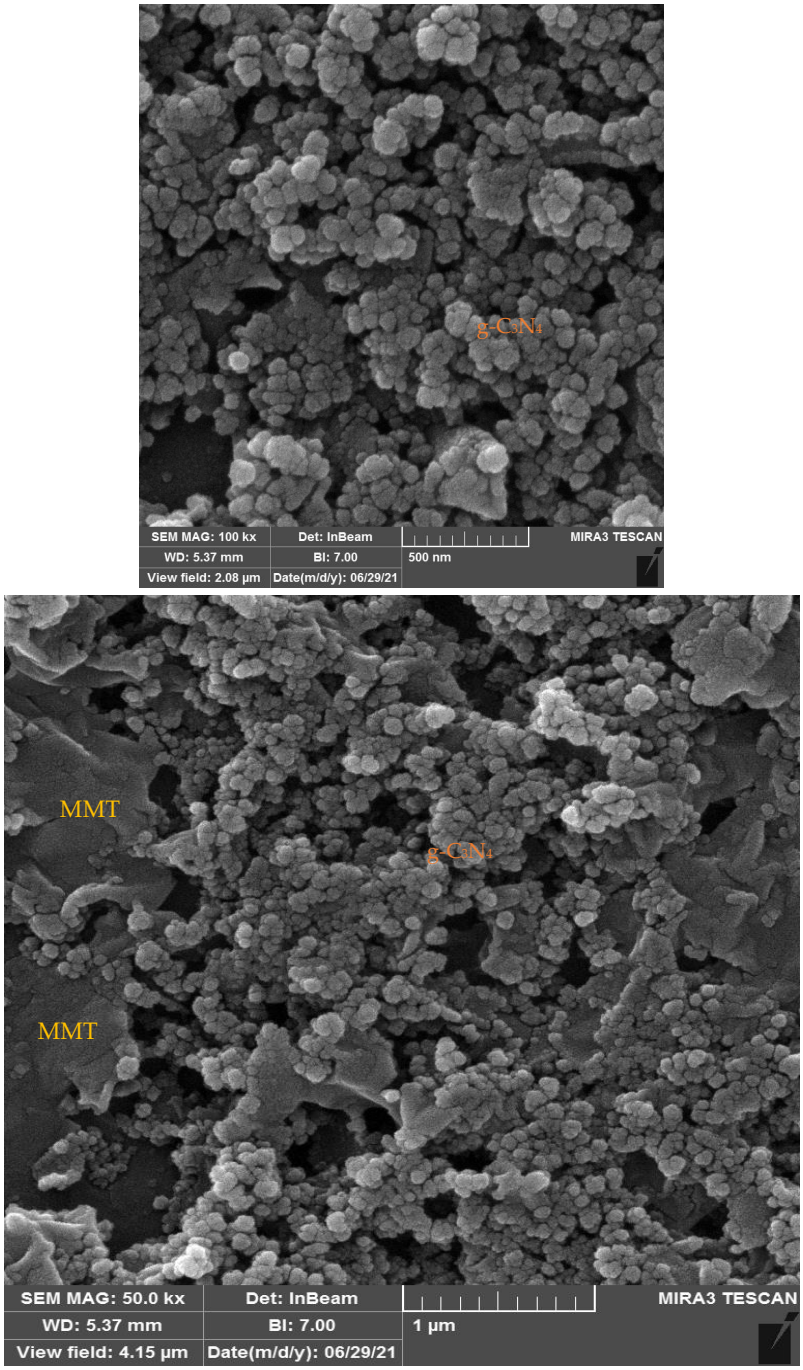

(**B**)

Figure 1. (**A**) TEM images of g-C_3N_4 and (**B**) FESEM images of MMT/g-C_3N_4. (**A**) The scale bar is at the bottom of right corner.

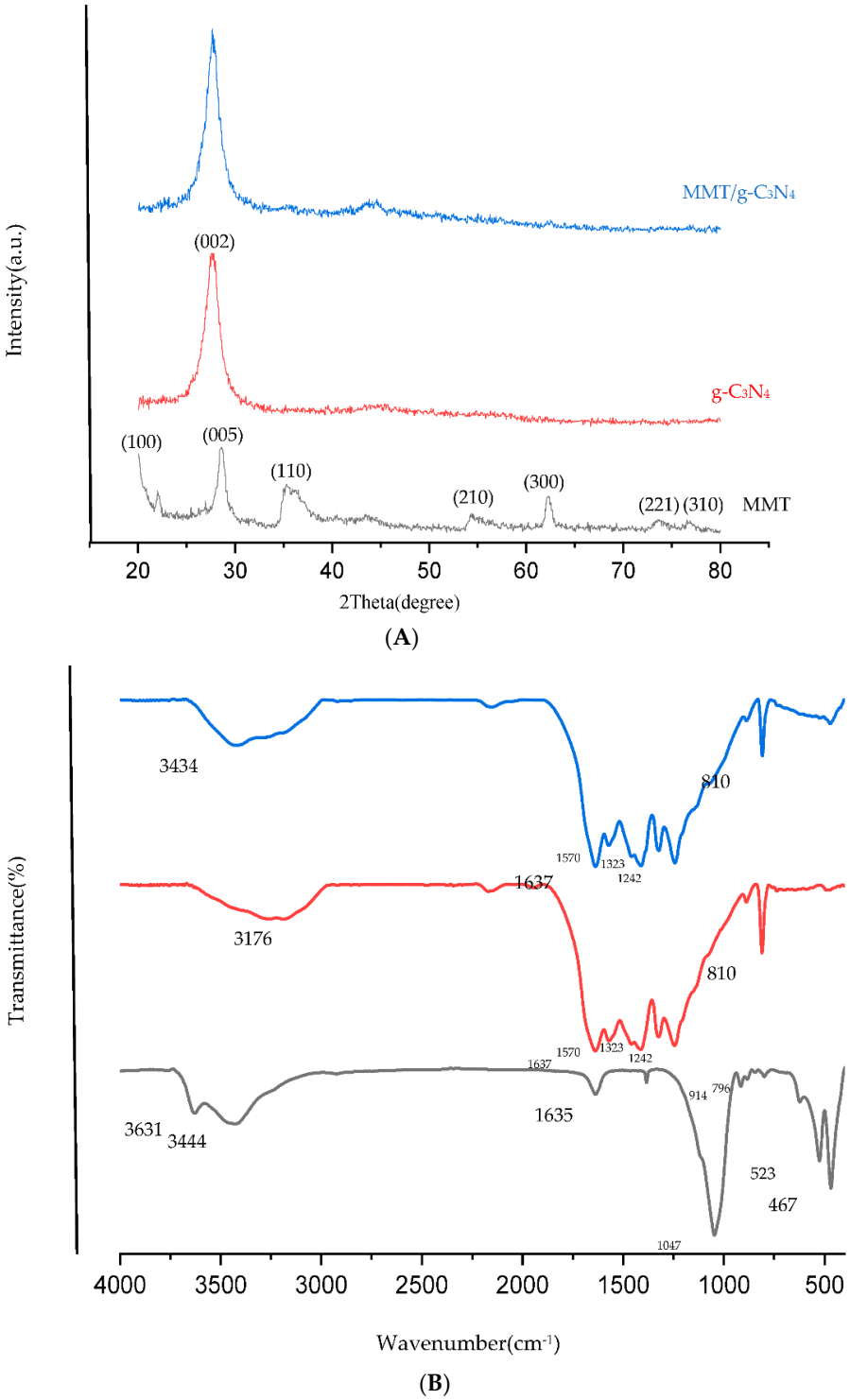

Figure 2. (**A**) The XRD patterns of the MMT, g-C_3N_4 and MMT/g-C_3N_4 and (**B**) the FTIR spectroscopy of the MMT, g-C_3N_4 and MMT/g-C_3N_4.

2.3. Optimization of Effective Operating Factors

2.3.1. In the Absence of the Nanostructure

A total of thirteen experimental runs of two factors (concentration of sulfur and cell concentration) were performed in duplicate with different combinations by applying CCD (Table 1).

Table 1. The results of CCD for two factors (concentration of sulfur and cell concentration) and the production of 2-HBP by *R.* sp. strain IGTS8.

Experimental Run	Concentration of Sulfur (Dibenzothiophene) (mM)	Cell Concentration (*v*/*v*)	Concentration of 2-HBP (mM)
1	0.15	1%	0.3
2	0.45	1%	0.38
3	0.15	3%	0.31
4	0.45	3%	0.4
5	0.15	2%	0.36
6	0.45	2%	0.38
7	0.3	1%	0.35
8	0.3	3%	0.33
9	0.3	2%	0.39
10	0.3	2%	0.38
11	0.3	2%	0.39
12	0.3	2%	0.39
13	0.3	2%	0.39

In the biodesulfurization studies, the concentration of DBT is typically expressed as mM, and due to this fact we did not convert mM to ppm. Parts per million is used to describe concentrations of highly diluted solutions, and we did not have a highly diluted solution.

2.3.2. In the Presence of the Nanostructure

A total of fifteen experimental runs of three factors (concentration of nanostructure (MMT/g-C_3N_4), concentration of sulfur (DBT) and cell concentration) were performed in duplicate with different combinations by applying CCD (Table 2).

Table 2. The results of CCD for three factors (concentration of nanostructure (MMT/g-C3N4), concentration of sulfur and cell concentration) and the production of 2-HBP by *R.* sp. strain IGTS8.

Experimental Run	Concentration of Nanostructure (MMT/g-C3N4) (mM)	Concentration of Sulfur (DBT) (mM)	Cell Concentration (*v*/*v*)	Concentration of 2-HBP (mM)
1	0.0005	0.15	1%	0.607
2	0.0015	0.15	1%	0.556
3	0.0005	0.45	1%	0.584
4	0.0015	0.45	1%	0.512
5	0.0005	0.15	3%	0.579
6	0.0015	0.15	3%	0.546
7	0.0005	0.45	3%	0.4
8	0.0015	0.45	3%	0.4
9	0.0005	0.3	2%	0.54
10	0.0015	0.3	2%	0.5
11	0.001	0.15	2%	0.5
12	0.001	0.45	2%	0.508
13	0.001	0.3	1%	0.599
14	0.001	0.3	3%	0.599
15	0.001	0.3	2%	0.56

2.4. Statistical Methods

2.4.1. Statistical Methods in the Absence of the Nanostructure

Analysis of variance was performed to investigate the effect of each factor, such as concentration of sulfur (DBT) and cell concentration, and also the interactions between these factors on biodesulfurization performance in the absence of the nanostructure (Table 3).

Table 3. ANOVA for evaluation of R_1 for *Rhodococcus erythropolis* IGTS8 in the absence of the nanostructure.

Source of Variance	The Sum of Squares Due to the Source (SS)	Degree of Freedom (df)	The Mean Sum of Squares Due to the Source (MS)	F Value	*p*-Value
Pattern	0.011	5	2.156×10^{-3}	6.43	0.0150 significant
A–A Concentration of sulfur (DBT)	6.017×10^{-3}	1	6.017×10^{-3}	17.96	0.0039
B–B Cell concentration	1.677×10^{-5}	1	1.677×10^{-5}	0.050	0.8299
AB	2.500×10^{-5}	1	2.500×10^{-5}	0.075	0.7926
A^2	8.941×10^{-5}	1	8.941×10^{-5}	0.27	0.6213
B^2	3.518×10^{-3}	1	3.518×10^{-3}	10.50	0.0142

The parameters that have *p*-values greater than 0.05 did not have a significant effect on the biodesulfurization activity of *Rhodococcus erythropolis* IGTS8. The *p*-values in the suggested pattern show positive and significant results (*p*-value < 0.05), and if the *p*-value is up to 0.0150 and the F value is up to 6.43, this means that the suggested pattern is very reasonable. The subsequent variables are important and effective in the R_1 response for *Rhodococcus erythropolis* IGTS8. The ultimate equation for the R_1 is as follows.

$$R_1 = 0.38 + 0.032A + 1.677 \times 10^{-3}B + 2.500 \times 10^{-3}AB - 5.690 \times 10^{-3}A^2 - 0.036B^2 \quad (1)$$

The obtained equation shows the relationship between the variables according to CCD and R_1. In this equation, the positive sign means the direct effect and the negative sign means the indirect effect of the independent variables on the R_1. In keeping with Equation (1), the optimum conditions for the R_1 response for *Rhodococcus erythropolis* IGTS8 in the absence of the nanostructure are shown in Table 4.

Table 4. Optimum conditions for R_1 response in the absence of the nanostructure.

A	B	R_1
Concentration of Sulfur (DBT)	**Cell Concentration**	**Concentration of 2-HBP**
0.80	−0.18	0.40437

In accordance with Equation (1) and Table 4, the interactions between the independent variables in optimum conditions are shown in Figure 3. This figure shows the interactions between the A (concentration of sulfur) and B (cell concentration) variables on the R_1 response (concentration of 2-HBP or biodesulfurization activity). Low cell concentrations and high concentrations of sulfur lead to the best biodesulfurization activity because a sufficient amount of sulfur is provided for the microorganism, and the bacterial growth is increased as a result of the access of the microorganism to the sulfur being increased. Only certain concentrations of sulfur are suitable for increasing the growth rate of the microorganism because there is a critical concentration of sulfur for the microorganism beyond which, at a higher concentration, it is toxic to the microorganism [23]. The consumption of sulfur and its high concentration result in the accumulation of 2-hydroxy biphenyl inside the cell,

and this has a toxic effect on cell growth, which does not have an appropriate effect on the biodesulfurization activity [21,51].

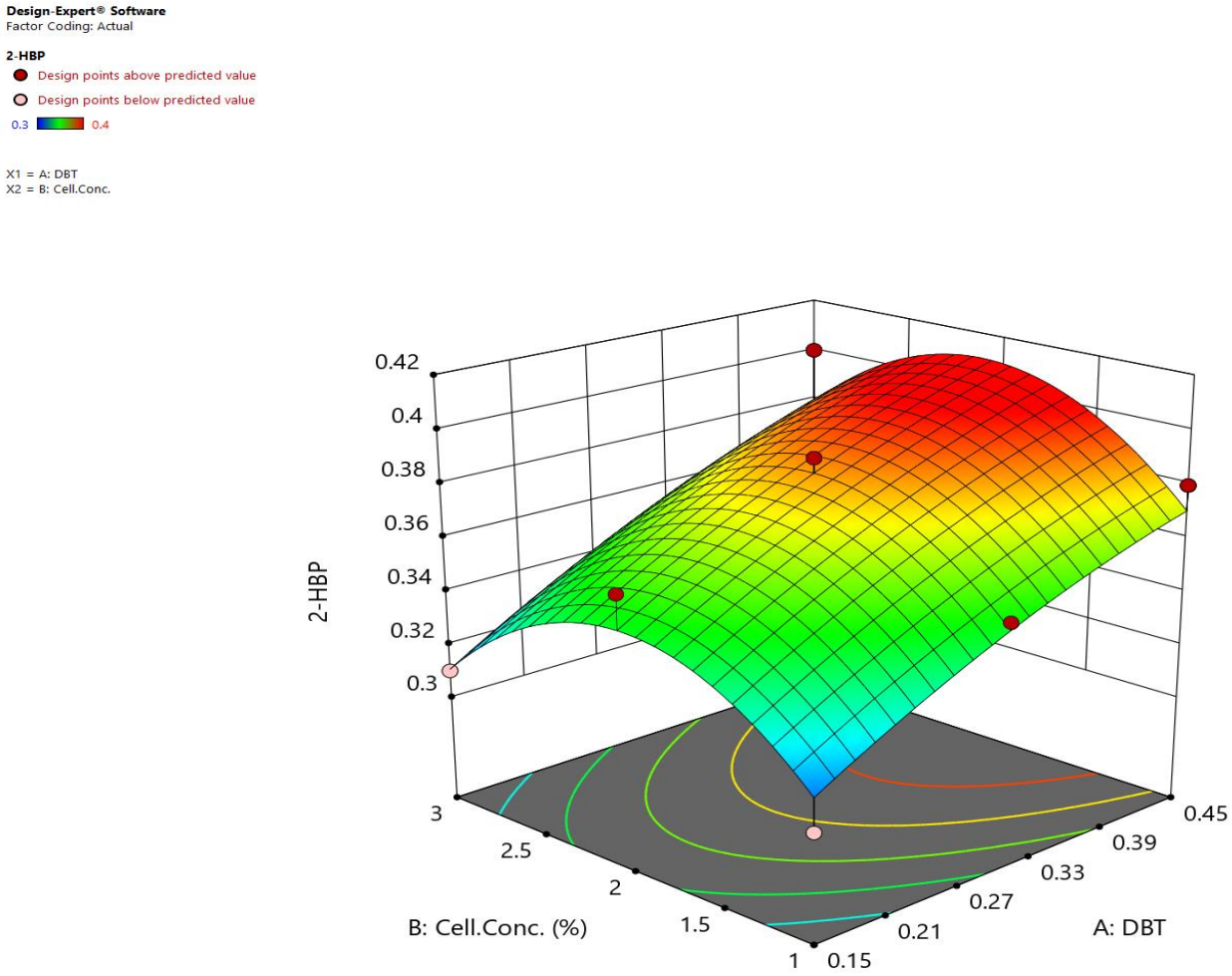

Figure 3. Three-dimensional plot of interactions of A: concentration of sulfur (dibenzothiophene) and B: cell concentration.

2.4.2. Statistical Methods in the Presence of the Nanostructure

Analysis of variance was performed to investigate the effect of each factor, such as concentration of nanostructure (MMT/g-C_3N_4), concentration of sulfur (DBT) and cell concentration, and also the interactions between these factors on the biodesulfurization performance in the presence of the nanostructure (Table 5).

The parameters that have *p*-values greater than 0.05 did not have a significant effect on the biodesulfurization activity of *Rhodococcus erythropolis* IGTS8. The *p*-values in the suggested pattern show positive and significant results (*p*-value < 0.05), and if the *p*-value is up to 0.0019 and the F value is up to 7.67, this means that the suggested pattern is very reasonable. The subsequent variables are important and effective in the R_1 response for *Rhodococcus erythropolis* IGTS8. The final equation for the R_1 is as follows.

$$R_1 = 0.56 - 0.020A - 0.038B - 0.033C + 1.500 \times 10^{-3}AB + 0.011AC - 0.032BC - 0.033A^2 - 0.049B^2 + 0.046C^2 \quad (2)$$

The obtained equation shows the relationship between the variables according to CCD and R_1. In this equation, the positive sign means the direct effect and the negative sign means the indirect effect of the independent variables on the R_1. In keeping with Equation (2), the optimum conditions for the R_1 response for *Rhodococcus erythropolis* IGTS8 in the presence of the nanostructure are shown in Table 6.

Table 5. ANOVA for evaluation of R_1 for *Rhodococcus erythropolis* IGTS8 in the presence of the nanostructure.

Sources of Variance	The Sum of Squares Due to the Source (SS)	Degree of Freedom (df)	The Mean Sum of Squares Due to the Source (MS)	F Value	*p*-Value
Pattern	0.054	9	5.998×10^{-3}	7.67	0.0019 significant
A–A Concentration of nanostructure (MMT/g-C_3N_4)	3.842×10^{-3}	1	3.842×10^{-3}	4.91	0.0510
B–B Concentration of sulfur (DBT)	0.015	1	0.015	18.85	0.0015
C–C Cell concentration	0.011	1	0.011	14.26	0.0036
AB	1.800×10^{-5}	1	1.800×10^{-5}	0.023	0.8824
AC	1.013×10^{-3}	1	1.013×10^{-3}	1.29	0.2818
BC	8.320×10^{-3}	1	8.320×10^{-3}	10.64	0.0086
A^2	2.945×10^{-3}	1	2.945×10^{-3}	3.77	0.0810
B^2	6.529×10^{-3}	1	6.529×10^{-3}	8.35	0.0161
C^2	5.888×10^{-3}	1	5.998×10^{-3}	7.53	0.0207

Table 6. Optimum conditions for R_1 response for *Rhodococcus erythropolis* IGTS8 in the presence of the nanostructure.

A	B	C	R_1
Concentration of Nanostructure (MMT/g-C3N4)	**Concentration of Sulfur (DBT)**	**Cell Concentration**	**Concentration of Produced 2-HBP**
−0.11	−0.13	−0.99	0.63808

In accordance with Equation (2) and Table 6, the interactions between the independent variables in optimum conditions are shown in Figure 4A–C. Figure 4A shows the interaction between A (concentration of nanostructure) and B (concentration of sulfur) variables on the R_1 response (concentration of 2-HBP or biodesulfurization activity). As can be seen, when the concentrations of the nanostructure and sulfur are at low levels, they show higher desulfurization rates compared with when the concentrations of the nanostructure and sulfur are at their high levels. The reason is that the high concentrations of the nanostructure reduce the growth rate of the microorganisms and also increase their lag phase [52]. Additionally, the microorganisms produce a surfactant; a sufficient amount of sulfur (DBT) is available to the microorganisms (even at low concentrations of sulfur). The mass transfer rate of sulfur compounds is very low and the nanostructure of the MMT/g-C_3N_4 as a new adsorbent increases the availability of organic sulfur compounds by adsorption to the microorganisms. Consequently, the nanostructure increases the permeability of the membrane and, in addition to increasing the transportation of sulfur into the microorganism, causes the transportation of 2-hydroxy biphenyl out of cell, thus improving the biodesulfurization activity [12].

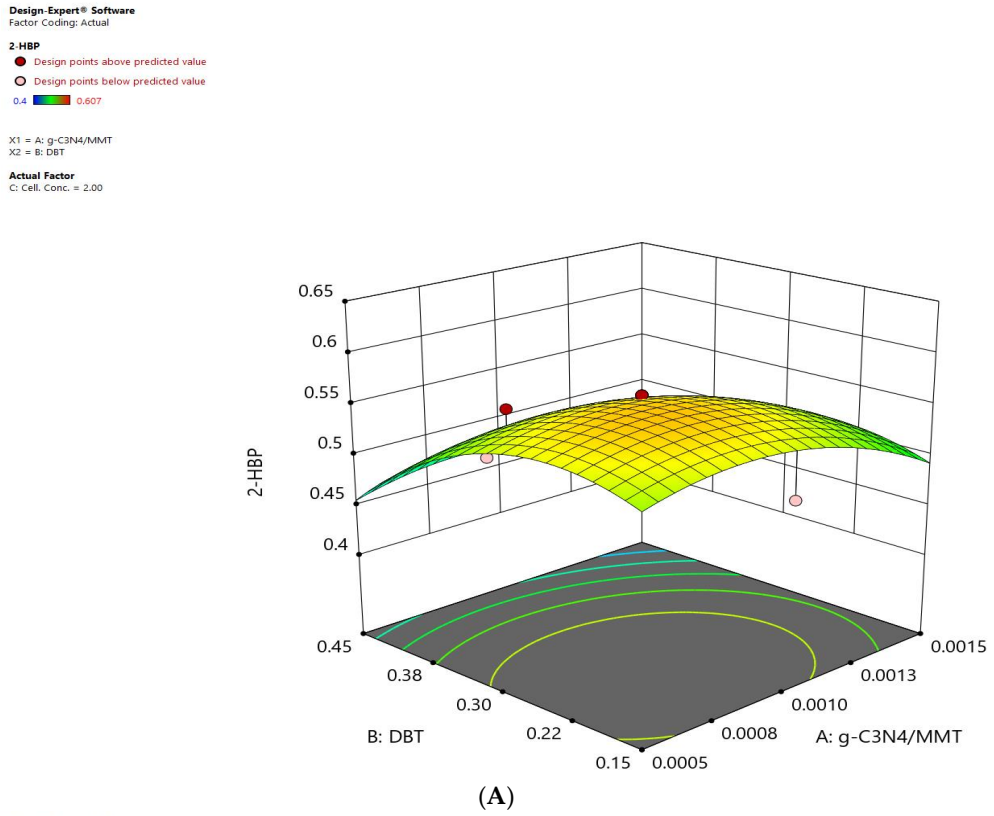

(**A**)

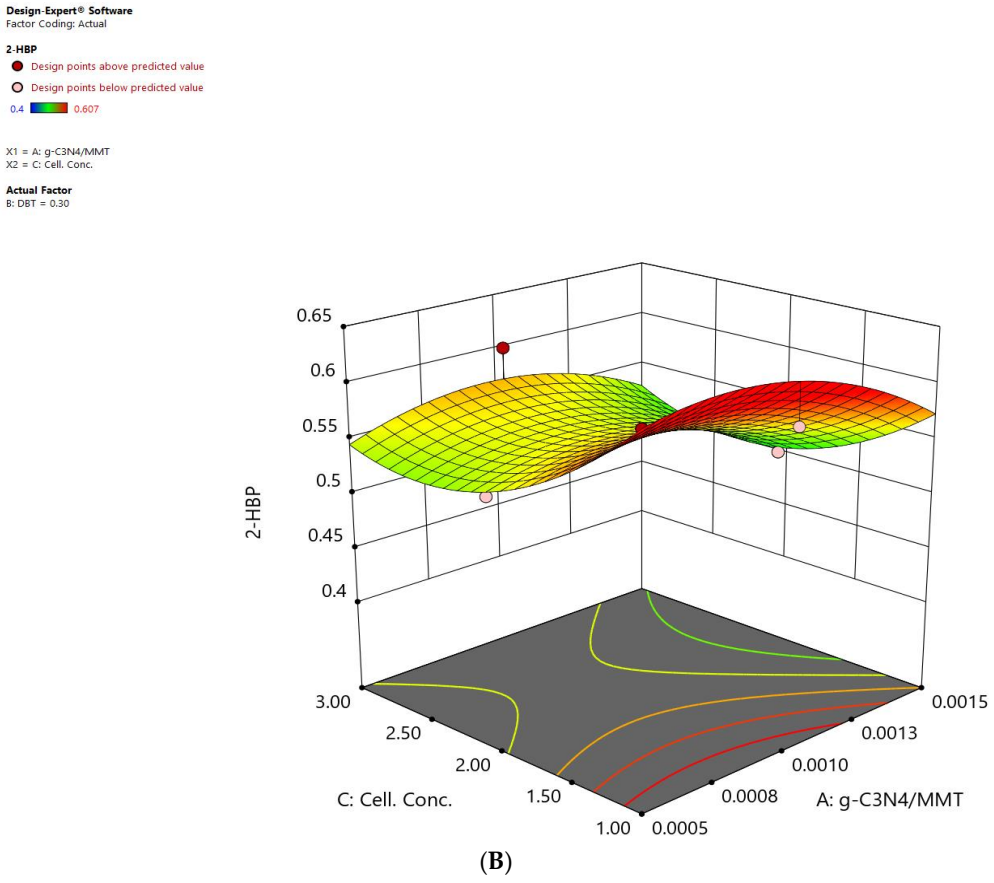

(**B**)

Figure 4. *Cont*.

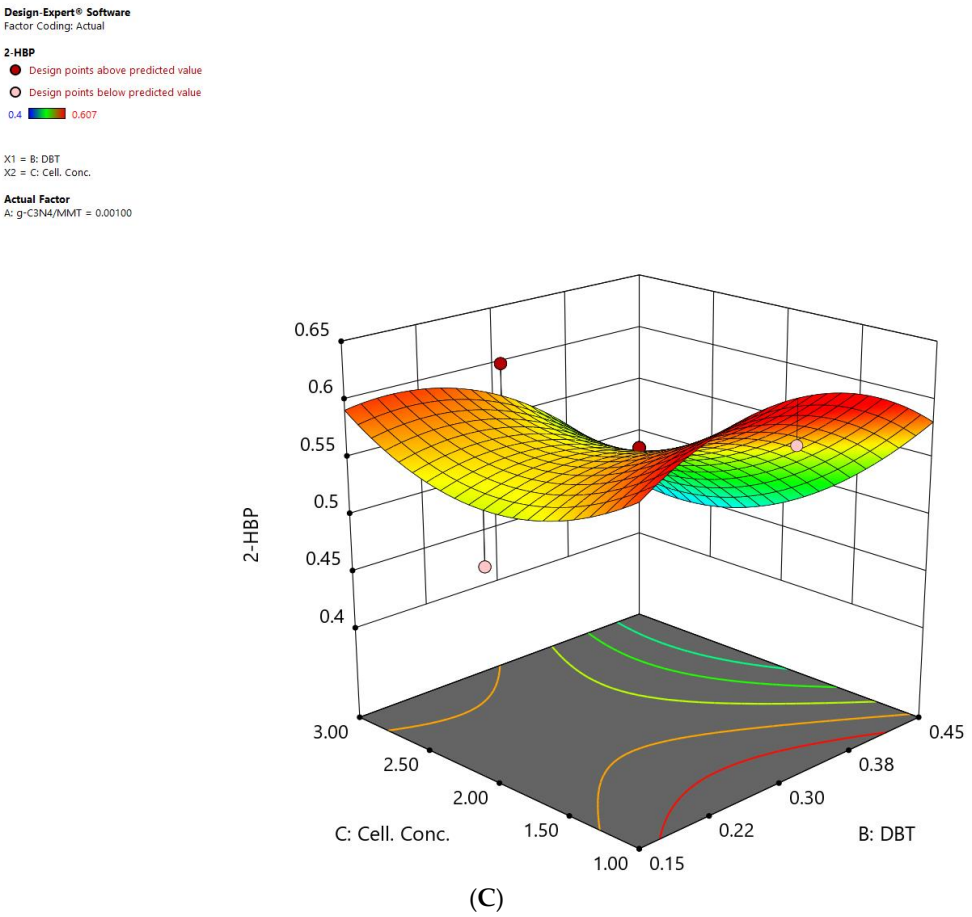

Figure 4. (**A**) Three-dimensional plot of interactions of A: concentration of nanostructure (MMT/g-C_3N_4) and B: concentration of sulfur (DBT). (**B**) Three-dimensional plot of interactions of A: concentration of nanostructure (MMT/g-C_3N_4) and C: cell concentration. (**C**) Three-dimensional plot of interactions of B: concentration of sulfur (DBT) and C: cell concentration.

In this case, if we provide a high amount of sulfur for the microorganism, it will reduce the biodesulfurization activity and the desired result will not be obtained.

Figure 4B shows the interactions between the A (concentration of nanostructure) and C (cell concentration) variables on the R_1 response (concentration of 2-HBP or biodesulfurization activity). As can be seen, when the concentration of the nanostructure and cell concentration are at low levels, they show higher desulfurization rates compared with when the concentrations of the nanostructure and cell are at their high levels. The reason is that even at low levels of concentration of the nanostructure, there is an effective transportation of sulfur (DBT). The nanostructure probably affects the permeability of the membrane and, in addition to increasing the transportation of sulfur into the microorganism, causes the transportation of 2-HBP out of cell, thus reducing the toxic effects of this substance.

Figure 4C shows the interactions between the B (concentration of sulfur (DBT)) and C (cell concentration) variables on the R_1 response (concentration of 2-HBP or biodesulfurization activity). As can be seen, when the concentration of sulfur (DBT) and cell concentration are at low levels, they show higher desulfurization rates compared with when the concentrations of the nanostructure and sulfur are at their high levels. In this case, thanks to the presence of the nanostructure, the effective transportation of sulfur (DBT) takes place. Furthermore, increasing the cell concentration results in the accumulation of cells at the interface, which prevents the uptake of sulfur and also the transfer of the required oxygen for the oxidation reaction within the 4S pathway [53]. This reduces the desulfurization activity. As a result, increasing the cell concentration does not cause further production of 2-HBP, and this does not increase the biodesulfurization activity.

2.5. Biodesulfurization Activity

The final product of the biodesulfurization of DBT is 2-HBP, which was identified by the Gibbs assay. The results during 248 h cycles are exhibited. In Figures 5 and 6, the results of the Gibbs assay show that the maximum extracellular concentration was 0.33 mM at t = 120 h for free cells and 0.99 mM for decorated cells during 248 h. The concentration of produced 2-HBP by the decorated cells was significantly increased compared with the nondecorated cells. An almost two-fold improvement in the biodesulfurization activity was obtained for the decorated cells compared with the free cells.

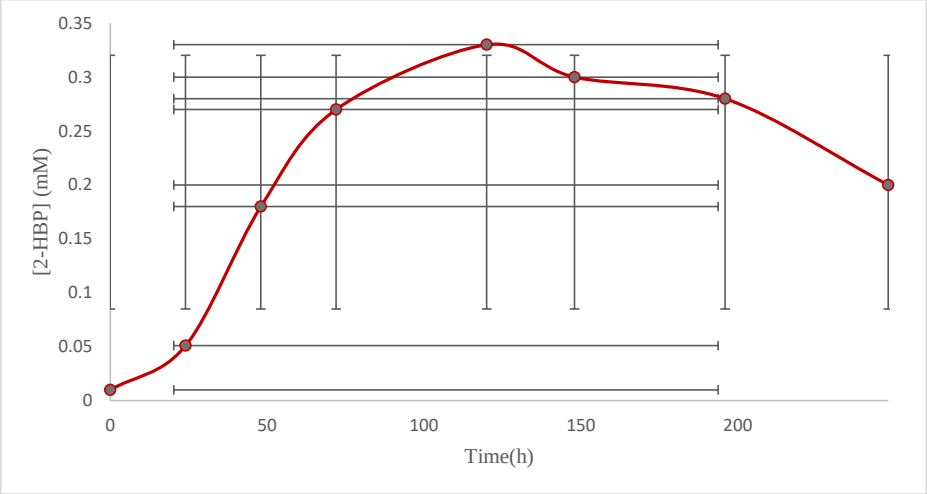

Figure 5. The concentration of produced 2-HBP by the nondecorated cells.

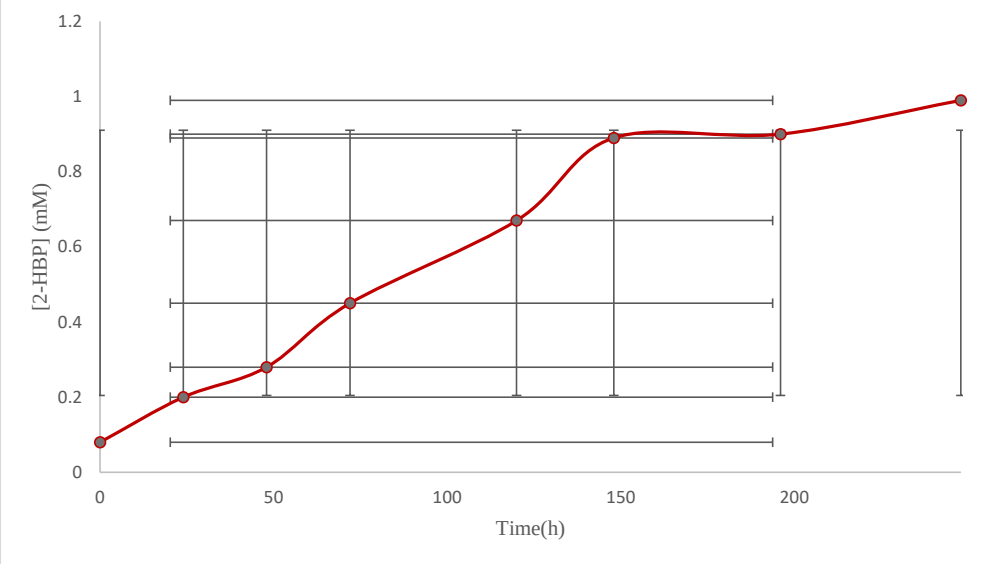

Figure 6. The concentration of produced 2-HBP by the decorated cells.

While biodesulfurization occurs in the cytoplasm, the surface of the bacteria limits the transportation of dibenzothiophene into the cell and the transportation of 2-hydroxy biphenyl out of the cell. Consequently, the nanostructure increases the permeability of the membrane and, in addition to increasing the transportation of sulfur into the microorganism, causes the transportation of 2-hydroxy biphenyl out of cell, thus improving the biodesulfurization efficiency [12].

In this study, due to a lack of time and a limited budget, we did not measure the DBT concentration after the biodesulfurization process.

3. Materials and Methods

3.1. Materials

Dibenzothiophene (99%), 2-hydroxy biphenyl and 2, 6-dichloroquinone-4-chloroimide (Gibbs reagent) were obtained from Sigma Aldrich. The rest of the required chemicals, such as urea and sodium boron hydride (sodium tetrahydroborate), were purchased in a suitable degree of decomposition from the reputable German company Merck.

3.2. The Microorganism and Its Medium

The microorganism used in this research was *Rhodococcus* sp. strain IGTS8, and it was collected from the RIPI (Research Institute of Petroleum Industry). In most of the biodesulfurization research, *Rhodococcus erythropolis* IGTS8 has been used because of its high activity and selectivity in removing sulfur from organic compounds in crude oil. In addition, because of the special structure of their cell walls and their appropriate biochemical characteristics for the biological degradation of organic compounds, these microbial cells have been used in this research, and they have also shown great potential for BDS.

In order to grow the microorganism, the basal salt medium (BSM) was used, and it had the following composition [12]: Na_2HPO_4 (5.47 g), NH_4Cl (2.00 g), KH_2PO_4 (2.44 g), $MgCl_2.6H_2O$ (0.20 g), $MnCl_2.4H_2O$ (0.004 g), $FeCl_3.6H_2O$ (0.001 g), $CaCl_2.2H_2O$ (0.001 g) and 1000 mL of deionized water with 2 mL of dissolved glycerol. The structure of *Rhodococcus erythropolis* IGTS8 was studied earlier [54].

3.3. Preparation of the Nanoparticles

3.3.1. Synthesis of Bulk Graphitic Carbon Nitride

There are various methods to synthesize graphitic carbon nitride, but basically bulk graphitic carbon nitride is acquired from the calcination of urea, thiourea, melamine and cyanamide [55]. The synthesis steps were as follows: First, 10 g of urea in powdered form was placed in a crucible. It was heated at 550 °C for 4 h in the muffle furnace (The heating rate was 5 °C/min), and a dull yellow powder was formed.

3.3.2. Synthesis of Graphitic Carbon Nitride Nanosheets

There are several methods to synthesize graphitic carbon nitride nanosheets. One of these methods is liquid exfoliation. Liquid exfoliation is used because its use of water as a solvent is environmentally friendly, and it results in the formation of nanosheets that have a high specific surface area. In 2015, Huang et al. used liquid exfoliation for synthesizing nanosheets of g-C_3N_4 [56]. Yuan et al. also synthesized graphitic carbon nitride nanosheets in 2019 in this way [57]. In 2019, Hatami et al. also used this method to synthesis graphitic carbon nitride nanosheets [58]. In this research, the nanosheets were synthesized using the method of Hatami et al. The synthesis steps were as follows: 75 mg of graphitic carbon nitride was added to 15 mL of distilled water and then placed in an ultrasonic bath for 30 min until a homogeneous graphitic carbon nitride solution (5 mg/mL) was synthesized.

3.3.3. Synthesis of Montmorillonite/Graphitic Carbon Nitride

A mix of 15 mL of graphitic carbon nitride (5 mg/mL) with 75 mg of montmorillonite was placed in an ultrasonic bath at 25° C and, after 30 min, 10 mg of sodium borohydride was added as a reductant to form a montmorillonite/graphitic carbon nitride solution at a concentration of 10 mg/mL.

3.4. Experimental Design

The concentration of the nanostructure (montmorillonite/graphitic carbon nitride), the concentration of sulfur (dibenzothiophene) and the cell concentration were contemplated as the major factors in biodesulfurization. In order to evaluate the optimal level of the major factors and their relationship in biodesulfurization efficiency, three levels of these three factors were applied in the central composite design (CCD).

3.5. Analytical Methods

3.5.1. Determination of Biodesulfurization Activity of Microorganisms (Gibbs Assay)

The final product of the biodesulfurization of dibenzothiophene is called 2-hydroxy biphenyl, which can be identified using the Gibbs assay [59]. In this study, we did not use an HPLC analysis because the HPLC system is rather expensive compared with other analytical tools, the analytical columns are expensive and have a relatively short operating life, the solvents are expensive and disposal of the used solvents is becoming a real problem. The bewildering number of HPLC modules, columns, mobile phases and operating parameters renders HPLC difficult for the novice. In this study, we did not use a GC-MS analysis because gas chromatography, though a dynamically developing analytical technique, involves disadvantages such as a long analysis time and the impossibility of real-time analysis or direct quantitative determinations. The basic constraints affecting its complementarity can be divided into three categories: limited selectivity, problems related to the chromatographic system's resolution, and the insufficient sensitivity of the MS detectors. The limitation of selectivity applies to various methods of sample preparation, so the result of the determinations may be unreliable and may not reflect the actual concentrations or compositions of the samples.

3.5.2. Characterization of Nanostructures

In order to investigate the shape and morphology of the nanoparticles, transmission electron microscopy (TEM) and FESEM images were taken. These images were investigated using TEM (Philips CM120) and FESEM (TESCAN MIRA III). FTIR (Thermo AVATAR) was used to examine the chemical structure of the nanostructures. XRD (Philips PW1730) was used to examine the crystal structure of the nanostructures. In this study, due to a limited budget and lack of time, four characterization methods were used.

3.6. Biodesulfurization Capacity of Decorated Microbial Cells in a Bioreactor

The microbial cells were cultured in a basal salt medium (BSM) until the mid-exponential growth phase and harvested by centrifugation at 1400 g for 10 min. Subsequently, the microbial cell pellets were washed twice with Ringer's solution and suspended in the basal salt medium (BSM) to A_{600} = 1. Following this, the microbial cells were decorated with the MMT/g-C_3N_4 nanostructure as follows: 20 mL of the suspension containing 5 mg/mL of MMT/g-C_3N_4 nanostructure per ml of water was mixed with 50 mL of the cell suspension in the basal salt medium (BSM) with DBT at a final concentration of 0.15 mM. The biodesulfurization activity of the microbial cells was evaluated in a stirring reactor (5 L) containing 2 L basal salt medium (BSM) using a Gibbs assay.

4. Conclusions

The synthesis and combining of MMT/g-C_3N_4 was achieved successfully. The g-C_3N_4 nanosheets covered the surface of the MMT (Figure 1B). The surface of the MMT was covered with the g-C_3N_4 uniformly. The MMT/g-C_3N_4 had a FTIR pattern analogous with that of the g-C_3N_4 nanosheets, confirming the proper bonding of the g-C_3N_4 nanosheets to the MMT/g-C_3N_4 (Figure 2B). The production rate of 2-hydroxy biphenyl before the use of the nanostructure (MMT/g-C_3N_4) was equal to 0.4 mM, while after the use of the nanostructure (MMT/g-C_3N_4) the production rate of 2-hydroxy biphenyl was equal to 0.607 mM, this result showing a 52% (51.75%) increase in the desulfurization process, which represents a very satisfactory result. This difference is probably due to the increasing microbial activity and membrane permeability in the presence of the nanostructure. The nanostructure facilitates the access to sulfur compounds of the microorganisms that cause the transportation of DBT into the cell and the removal of 2-HBP from cell. The concentration of sulfur (DBT) was the only parameter that affected the biodesulfurization process. R-squared was equal to 0.8213, which means that the presented regression model was more than 82% consistent with the experimental data. This is a good result, indicating a high correlation and good fit of the data (Table 3). The concentration of the nanostructure,

concentration of sulfur (DBT) and cell concentration were the three parameters that affected the biodesulfurization process. R-Squared was equal to 0.8734, which means that the proposed regression model was more than 87% consistent with the experimental data. This is a good result, indicating a high correlation and good fit of the data (Table 5). In order to compare our findings with other studies, Table 7 is given. The comparison of our findings with the results of other studies in Table 7 shows that the results of the present study are an acceptable achievement. The montmorillonite/graphitic carbon nitride nanostructure increases the efficiency of biodesulfurization.

Table 7. Comparison of the results of research in the field of biodesulfurization.

Strain	Nanoparticle	The Increase in Biodesulfurization Efficiency	Reference
Pseudomonas delafieldii	Magnetite nanoparticles (Fe_3O_4)	-	[20]
Rhodococcus erythropolis LSSE8-1	Magnetite nanoparticles (Fe_3O_4)	-	[60]
Rhodococcus erythropolis LSSE8-1-vgb	Nano-γ-Al_2O_3	20%	[22]
Rhodococcus erythropolis FMF and *R. erythropolis* IGTS8	Fe_3O_4	-	[13]
Rhodococcus erythropolis IGTS8	Magnetic Fe_3O_4 nanoparticles	15.3%	[12]
Pseudomonas aeroginusa PTSOX4	ZnO	1.4-fold (40%)	[24]
Rhodococcus erythropolis IGTS8	Modified carbon nanotube	12%	[52]
Bacillus thermoamylovorance strain EAMYO	Starch/iron nanoparticles	For Fe^0/starch it was increased by about 26.52% and for Fe_3O_4/starch it was increased by about 10.75%	[61]
Rhodococcus erythropolis IGTS8	Starch/Fe_3O_4	50%	[62]
Rhodococcus sp. FUM94	-	Not mentioned	[53]
Gordonia sp.	-	Not mentioned	[63]
Rhodococcus erythropolis IGTS8	MMT/g-C_3N_4	52%	This study

In Figures 5 and 6, the results of the Gibbs assay showed that the maximum extracellular concentration was 0.33 mM at t = 120 h for free cells and 0.99 mM for decorated cells during 248 h. The production rate of 2-HBP by decorated cells was significantly increased compared with nondecorated cells. An almost two-fold improvement in biodesulfurization activity was obtained for decorated cells compared with free cells.

Author Contributions: N.Y.H., M.P.: Conceptualization, writing—original draft preparation, A.G., F.Y., A.R. and G.Z.K.; Supervision, and project administration, F.Y. All authors have read and agreed to the published version of the manuscript.

Funding: This research received no external funding.

Data Availability Statement: The data included into the text.

Conflicts of Interest: The authors declare no conflict of interest.

References

1. Gupta, N.; Roychoudhury, P.K.; Deb, J.K. Biotechnology of desulfurization of diesel: Prospects and challenges. *Appl. Microbiol. Biotechnol.* **2005**, *66*, 356–366. [CrossRef] [PubMed]
2. Shavandi, M.; Sadeghizadeh, M.; Khajeh, K.; Mohebali, G.; Zomorodipour, A. Genomic structure and promoter analysis of the dsz operon for dibenzothiophene biodesulfurization from *Gordonia alkanivorans* RIPI90A. *Appl. Microbiol. Biotechnol.* **2010**, *87*, 1455–1461. [CrossRef] [PubMed]
3. Sohrabi, M.; Kamyab, H.; Janalizadeh, N.; Huyop, F.Z. Bacterial Desulfurization of Organic Sulfur Compounds Exist in Fossil Fuels. *J. Pure Appl. Microbiol.* **2012**, *6*, 717–729.

4. Soleimani, M.; Bassi, A.; Margaritis, A. Biodesulfurization of refractory organic sulfur compounds in fossil fuels. *Biotechnol. Adv.* **2007**, *25*, 570–596. [CrossRef]
5. Sousa, J.P.M.; Neves, R.; Sousa, S.F.; Ramos, M.J.; Fernandes, P. Reaction Mechanism and Determinants for Efficient Catalysis by DszB, a Key Enzyme for Crude Oil Bio-desulfurization. *ACS Catal.* **2020**, *10*, 9545–9554. [CrossRef]
6. Mohebali, G.; Ball, A.S. Biodesulfurization of diesel fuels—Past, present and future perspectives. *Int. Biodeterior. Biodegrad.* **2016**, *110*, 163–180. [CrossRef]
7. Sadare, O.O.; Obazu, F.; Daramola, M.O. Biodesulfurization of Petroleum Distillates—Current Status, Opportunities and Future Challenges. *Environments* **2017**, *4*, 85. [CrossRef]
8. Alves, L.; Marques, S.; Matos, J.; Tenreiro, R.; Gírio, F.M. Dibenzothiophene desulfurization by *Gordonia alkanivorans* strain 1B using recycled paper sludge hydrolyzate. *Chemosphere* **2008**, *70*, 967–973. [CrossRef]
9. Mohebali, G.; Ball, A.S. Biocatalytic desulfurization (BDS) of petro diesel Fuels. *Microbiology* **2008**, *154*, 2169–2183. [CrossRef]
10. Mohebali, G.; Ball, A.S.; Rasekh, B.; Kaytash, A. Biodesulfurization potential of a newly isolated bacterium *Gordonia alkanivorans* RIPI90A. *Enzym. Microb. Technol.* **2007**, *40*, 578–584. [CrossRef]
11. Rahpeyma, S.S.; Dilmaghani, A.; Raheb, J. Evaluation of desulfurization activity of SPION nanoparticle-coated bacteria in the presence of magnetic field. *Appl. Nanosci.* **2018**, *8*, 1951–1972. [CrossRef]
12. Karimi, E.; Jeffryes, C.; Yazdian, F.; Akhavan Sepahi, A. DBT desulfurization by decorating *Rhodococcus erythropolis* IGTS8 using magnetic Fe_3O_4 nanoparticles in a bioreactor. *Eng. Life Sci.* **2016**, *17*, 528–535. [CrossRef] [PubMed]
13. Bardania, H.; Raheb, J.; Mohammad-Beigi, H.; Rasekh, B.; Arpanaei, A. Desulfurization activity and reusability of magnetite nanoparticle–coated *Rhodococcus erythropolis* FMF and *R. erythropolis* IGTS8 bacterial cells. *Biotechnol. Appl. Biochem.* **2013**, *60*, 323–329. [CrossRef]
14. Bell, K.S.; Philp, J.C.; Aw, D.W.J.; Christofi, N. The genus *Rhodococcus*. *J. Appl. Microbiol.* **1998**, *85*, 195–210. [CrossRef]
15. Karimi, E.; Yazdian, F.; Rasekh, B.; Akhavan Sepahy, A. Biodesulfurization of Dibenzothiophene by *Rhodococcus erythropolis* IGTS8 in the Presence of Magnetic Nanoparticles and Carbon Nanotubes Surface modified Polyethylene Glycol. *Modares J. Biotechnol.* **2018**, *9*, 301–308.
16. Prasoulas, G.; Dimos, K.; Glekas, P.; Kalantzi, S.; Sarris, S.; Templis, C.; Vavitsas, K.; Hatzinikolaou, D.G.; Papayannakos, N.; Kekos, D.; et al. Biodesulfurization of Dibenzothiophene and Its Alkylated Derivatives in a Two-Phase Bubble Column Bioreactor by Resting Cells of *Rhodococcus erythropolis* IGTS8. *Processes* **2021**, *9*, 2064. [CrossRef]
17. Etemadi, N.; Akhavan Sepahi, A.; Mohebali, G.; Yazdian, F. The Isolation Desulfurizing Native Thermophilic Bacteria *Bacillus thermoamylovorance* and Optimization Culture Medium. *J. Pet. Res.* **2019**, *29*, 119–131.
18. Monticello, D.; Finnerty, W. Microbial desulfurization of fossil fuels. *Annu. Rev. Microbiol.* **1985**, *39*, 371–389. [CrossRef]
19. Wang, W.; Ma, T.; Lian, K.; Zhang, Y.; Tian, H.; Ji, K.; Li, G. Genetic Analysis of Benzothiophene Biodesulfurization Pathway of *Gordonia terrae* Strain C-6. *PLoS ONE* **2013**, *8*, e84386. [CrossRef]
20. Shan, G.; Xing, J.; Zhang, H.; Liu, H. Biodesulfurization of dibenzothiophene by microbial cells coated with magnetite nanoparticles. *Appl. Environ. Microbiol.* **2005**, *71*, 4497–4502. [CrossRef]
21. Ansari, F.; Grigoriev, P.; Libor, S.; Tothill, I.E.; Ramsden, J.J. DBT degradation enhancement by decorating *Rhodococcus erythropolis* IGST8 with magnetic Fe_3O_4 nanoparticles. *Biotechnol. Bioeng.* **2009**, *102*, 1505–1512. [CrossRef] [PubMed]
22. Zhang, T.; Li, W.-L.; Chen, X.-X.; Tang, H.; Li, Q.; Xing, J.-M.; Liu, H.-Z. Enhanced biodesulfurization by magnetic immobilized *Rhodococcus erythropolis* LSSE8-1-vgb assembled with nano-γ-Al_2O_3. *World J. Microbiol. Biotechnol.* **2011**, *27*, 299–305. [CrossRef]
23. Etemadi, N.; Sepahy, A.A.; Mohebali, G.; Yazdian, F.; Omidi, M. Enhancement of bio-desulfurization capability of a newly isolated thermophilic bacterium using starch/iron nanoparticles in a controlled system. *Int. J. Biol. Macromol.* **2018**, *120*, 1801–1809. [CrossRef] [PubMed]
24. Rahpeyma, S.S.; Mohammadi, M.; Raheb, J. Biodesulfurization of dibenzothiophene by two bacterial strains in cooperation with Fe_3O_4, ZnO and CuO nanoparticles. *J. Microb. Biochem. Technol.* **2017**, *9*, 587–591.
25. Canales, C.; Eyzaguirre, J.; Baeza, P.; Aballay, P.; Ojeda, J. Kinetic Analysis for Biodesulfurization of Dibenzothiophene Using *R. rhodochrous* Adsorbed on Silica. *Ecol. Chem. Eng. S* **2018**, *25*, 549–556. [CrossRef]
26. Nassar, H.N.; Abu Amr, S.S.; El-Gendy, N.S. Biodesulfurization of refractory sulfur compounds in petrodiesel by a novel hydrocarbon tolerable strain *Paenibacillus glucanolyticus* HN4. *Environ. Sci. Pollut. Res.* **2021**, *28*, 8102–8116. [CrossRef]
27. Ahmad, W.; Ahmad, I.; Ishaq, M.; Ihsan, K. Adsorptive desulfurization of kerosene and diesel oil by Zn impregnated montmorollonite clay. *Arab. J. Chem.* **2017**, *10*, S3263–S3269. [CrossRef]
28. Jia, C.; Zhang, M.; Lu, P. Preparation and characterization of polyurethane-/MMT nanocomposite-coated urea as controlled release fertilizers. *Polym.-Plast. Technol. Mater.* **2020**, *59*, 975–984. [CrossRef]
29. Feng, R.; Zhang, Y.; Li, H.; Wu, D.; Xin, X.; Zhang, S.; Yu, H.; Wei, Q.; Du, B. Ultrasensitive electrochemical immunosensor for zeranol detection based on signal amplification strategy of nanoporous gold films and nano-montmorillonite as labels. *Anal. Chim. Acta* **2013**, *758*, 72–79. [CrossRef]
30. Haseli, S.; Pourmadadi, M.; Samadi, A.; Yazdian, F.; Abdouss, M.; Rashedi, H.; Navaei-Nigjeh, M. A novel pH-responsive nanoniosomal emulsion for sustained release of curcumin from a chitosan-based nanocarrier: Emphasis on the concurrent improvement of loading, sustained release, and apoptosis induction. *Biotechnol. Prog.* **2022**, *38*, e3280. [CrossRef]
31. Ahmadi, M.; Pourmadadi, M.; Ghorbanian, S.A.; Yazdian, F.; Rashedi, H. Ultra pH-sensitive nanocarrier based on Fe_2O_3/chitosan/montmorillonite for quercetin delivery. *Int. J. Biol. Macromol.* **2021**, *191*, 738–745. [CrossRef] [PubMed]

32. Nazir, M.S.; Kassim, M.H.M.; Mohapatra, L.; Gilani, M.A.; Raza, M.R.; Majeed, K. Characteristic Properties of Nanoclays and Characterization of Nanoparticulates and Nanocomposites. In *Nanoclay Reinforced Polymer Composites*; Springer: Singapore, 2016; pp. 35–55. [CrossRef]
33. Takabatake, M.; Motokura, K. Montmorillonite-based heterogeneous catalysts for efficient organic reactions. *Nano Express* **2022**, *3*, 014004. [CrossRef]
34. Pielichowski, K.; Majka, T.M. (Eds.) *Polymer Composites with Functional Nanoparticles: Synthesis, Properties, and Applications*; Woodhead Publishing: Thorston, UK, 2019.
35. Zhang, Y.; Miao, B.; Chen, Q.; Bai, Z.; Cao, Y.; Davaa, B. Synthesis, Structure, and Photocatalytic Activity of TiO_2-Montmorillonite Composites. *Catalysts* **2022**, *12*, 486. [CrossRef]
36. Park, Y.; Ayoko, G.A.; Frost, R.L. Characterisation of organoclays and adsorption of p-nitrophenol: Environmental application. *J. Colloid Interface Sci.* **2011**, *360*, 440–456. [CrossRef] [PubMed]
37. Liu, B.; Wang, X.; Yang, B.; Sun, R. Rapid modification of montmorillonite with novel cationic Gemini surfactants and its adsorption for methyl orange. *Mater. Chem. Phys.* **2011**, *130*, 1220–1226. [CrossRef]
38. Zhou, Q.; Deng, S.; Yu, Q.; Zhang, Q.; Yu, G.; Huang, J.; He, H. Sorption of perfluorooctane sulfonate on organo-montmorillonites. *Chemosphere* **2010**, *78*, 688–694. [CrossRef]
39. Tiwari, R.R.; Khilar, K.C.; Natarajan, U. Synthesis and characterization of novel organo-montmorillonites. *Appl. Clay Sci.* **2008**, *38*, 203–208. [CrossRef]
40. Rezvani, M.A.; Khandan, S. Synthesis and characterization of a new nanocomposite (FeW_{11} V@CTAB-MMT) as an efficient heterogeneous catalyst for oxidative desulfurization of gasoline. *Appl. Organomet. Chem.* **2018**, *32*, e4524. [CrossRef]
41. Wang, C.; Zhu, W.; Xu, Y.; Xu, H. Preparation of TiO_2/g-C_3N_4 composites and their application in photocatalytic oxidative desulfurization. *Ceram. Int.* **2014**, *40*, 11627–11635. [CrossRef]
42. Zhao, R.; Li, X.; Su, J.; Gao, X. Preparation of WO_3/g-C_3N_4 composites and their application in oxidative desulfurization. *Appl. Surf. Sci.* **2017**, *392*, 810–816. [CrossRef]
43. Alaghmandfard, A.; Ghandi, K. A Comprehensive Review of Graphitic Carbon Nitride (g-C_3N_4)–Metal Oxide-Based Nanocomposites: Potential for Photocatalysis and Sensing. *Nanomaterials* **2022**, *12*, 294. [CrossRef] [PubMed]
44. Alnassar, M.A.; Alshehri, A.; Narasimharao, K. Visible Light Active Magnesium Silicate–Graphitic Carbon Nitride Nanocomposites for Methylene Blue Degradation and Pb^{2+} Adsorption. *Catalysts* **2022**, *12*, 1256. [CrossRef]
45. Ong, W.J.; Tan, L.L.; Ng, Y.H.; Yong, S.T.; Chai, S.P. Graphitic Carbon Nitride (g-C_3N_4)-Based Photocatalysts for Artificial Photosynthesis and Environmental Remediation: Are We a Step Closer to Achieving Sustainability? *Chem. Rev.* **2016**, *116*, 7159–7329. [CrossRef] [PubMed]
46. Seza, A.; Soleimani, F.; Naseri, N.; Soltaninejad, M. Novel microwave-assisted synthesis of porous g-C_3N_4/SnO_2 nanocomposite for solar water-splitting. *Appl. Surf. Sci.* **2018**, *440*, 153–161. [CrossRef]
47. Lin, Q.; Li, H.; Wang, X.; Jian, L.; Ren, J.; Liu, C.; Sun, R. SO_4^{2-}/Sn-MMT Solid Acid Catalyst for Xylose and Xylan Conversion into Furfural in the Biphasic System. *Catalysts* **2017**, *7*, 118. [CrossRef]
48. Qamar, M.A.; Shahid, S.; Javed, M.; Iqbal, S. Highly efficient g-C_3N_4/Cr-ZnO nanocomposites with superior photo-catalytic and antibacterial activity. *J. Photochem. Photobiol. A Chem.* **2020**, *401*, 112776. [CrossRef]
49. Shehap, A.; Nasr, R.; Mahfouz, M.A.; Ismail, A. Preparation and characterizations of high doping chitosan/MMT nanocomposites films for removing iron from ground water. *J. Environ. Chem. Eng.* **2021**, *9*, 104700. [CrossRef]
50. Choudhary, N.; Yadav, V.K.; Yadav, K.K.; Almohana, A.I.; Almojil, S.F.; Gnanamoorthy, G.; Kim, D.-H.; Islam, S.; Kumar, P.; Jeon, B.-H. Application of Green Synthesized MMT/Ag Nanocomposite for Removal of Methylene Blue from Aqueous Solution. *Water* **2021**, *13*, 3206. [CrossRef]
51. Zhang, L.; Dong, Y.; Wang, M.; Shi, S. Biodesulfurization of dibenzothiophene and other organic sulfur compound by newly isolated *Micobacterium* strain ZD-M2. *FEMS Microbiol. Lett.* **2005**, *247*, 45–50.
52. Karimi, E.; Yazdian, F.; Rasekh, B.; Jeffryes, C.; Rashedi, H.; Sepahi, A.A.; Shahmoradi, S.; Omidi, M.; Azizi, M.; Bidhendi, M.E.; et al. DBT desulfurization by decorating bacteria using modified carbon nanotube. *Fuel* **2018**, *216*, 787–795. [CrossRef]
53. Hokmabadi, M.; Khosravinia, S.; Mahdavi, M.A.; Gheshlaghi, R. Enhancing the biodesulphurization capacity of *Rhodococcus* sp. FUM94 in a biphasic system through optimization of operational factors. *J. Appl. Microbiol.* **2022**, *132*, 3461–3475. [CrossRef] [PubMed]
54. Ahmadi, N.N.; Hassani, K.H.; Kazemzad, M.; Ghavi, P.F.; Davoodi, D.F. Improvement of Desulfurization Performance of *Rhodococcus erythropolis* IGTS8 by Assembling Spherical Mesoporous Silica Nanosorbents on the Surface of the Bacterial Cells. *J. Appl. Chem. Res.* **2015**, *9*, 81–91.
55. Rono, N.; Kibet, J.K.; Martincigh, B.S.; Nyamori, V.O. A review of the current status of graphitic carbon nitride. *Crit. Rev. Solid State Mater. Sci.* **2021**, *46*, 189–217. [CrossRef]
56. Zhang, M.; Lai, C.; Li, B.; Huang, D. Rational Design 2D/2D Biobr/Cds/g-C_3N_4 Z-Scheme Heterojunction Photocatalyst with Carbon Dots as Solid-State Electron Mediators for Enhanced Visible and Nir Photocatalytic Activity: Kinetics, Inter-mediates, and Mechanism Insight. *J. Catal.* **2019**, *369*, 469–481. [CrossRef]
57. Talapaneni, S.N.; Lee, J.H.; Je, S.H.; Buyukcakir, O.; Kwon, T.-W.; Polychronopoulou, K.; Choi, J.W.; Coskun, A. Chemical Blowing Approach for Ultramicroporous Carbon Nitride Frameworks and Their Applications in Gas and Energy Storage. *Adv. Funct. Mater.* **2017**, *27*, 1604658. [CrossRef]

58. Sun, S.; Li, J.; Cui, J.; Gou, X.; Yang, Q.; Jiang, Y.; Liang, S.; Yang, Z. Simultaneously engineering K-doping and exfoliation into graphitic carbon nitride (g-C_3N_4) for enhanced photocatalytic hydrogen production. *Int. J. Hydrogen Energy* **2019**, *44*, 778–787. [CrossRef]
59. Mohamed, M.E.-S.; Al-Yacoub, Z.H.; Vedakumar, J.V. Biocatalytic desulfurization of thiophenic compounds and crude oil by newly isolated bacteria. *Front. Microbiol.* **2015**, *6*, 112. [CrossRef] [PubMed]
60. Li, Y.G.; Gao, H.S.; Li, W.L.; Xing, J.M.; Liu, H.Z. In situ magnetic separation and immobilization of *dibenzothio-phene-desulfurizing bacteria*. *Bioresour. Technol.* **2009**, *100*, 5092–5096. [CrossRef]
61. Etemadi, N.; Akhavan Sepahi, A.; Yazdian, F.; Mohebali, G. The Optimization of Culture Medium *Bacillus thermoamylovorance* Strain EAMYO by RSM and Improvement Biodesulfurization Activity by Starch/Iron Nano Particles. *J. Biotechnol.* **2020**, *11*, 127–136.
62. Sabaghian, S.; Yazdian, F.; Rasekh, B.; Shekarriz, M.; Mansouri, N. Investigating the effect of starch/Fe_3O_4 nanoparticles on biodesulfurization using molecular dynamic simulation. *Environ. Sci. Pollut. Res.* **2020**, *27*, 1667–1676. [CrossRef]
63. Kalita, M.; Chutia, M.; Jha, D.K.; Subrahmanyam, G. Mechanistic Understanding of *Gordonia* sp. in Biodesulfurization of Organosulfur Compounds. *Curr. Microbiol.* **2022**, *79*, 82. [CrossRef] [PubMed]